Characterizing Global & Regional Cardiac Diffusion Tensor Imaging Metrics in Healthy Subjects

Ariel J. Hannum[1,2,3,4](✉), Tyler E. Cork[1,2,3,4], Luigi E. Perotti[5], and Daniel B. Ennis[1,2,3,4]

[1] Department of Radiology, Stanford University, Stanford, CA, United States
ahannum@stanford.edu
[2] Division of Radiology, Veterans Administration Health Care System, Palo Alto, CA, United States
[3] Cardiovascular Institute, Stanford University, Stanford, CA, United States
[4] Department of Bioengineering, Stanford University, Stanford, CA, United States
[5] Department of Mechanical and Aerospace Engineering, University of Central Florida, Orlando, FL, United States

Abstract. Cardiac diffusion tensor imaging (cDTI) is an MRI technique used to characterize myocardial microstructure. Key metrics including mean diffusivity (MD), fractional anisotropy (FA), and helix angle pitch (HAP) have shown relevance in detecting microstructural remodeling. Herein, we aim to establish healthy baseline metrics for this emerging technique. To do so we assess average global cDTI metrics in the left ventricle for a cohort of healthy subjects (N=46) at 3 Tesla (T) with a single-shot echo-planar imaging (EPI) sequence. We hypothesize: (1) that there are no significant differences in cDTI metrics for groups within this population; and (2) that there are no significant differences between global, regional, and group-wide median values. To assess differences in global and regional cDTI metrics between groups, a one-way ANOVA test (for normal distributions) or Kruskal-Wallis test (for non-normal distributions) was performed to detect significance in cDTI metrics between four population groups: (1) Male $<$ 40 years old (yo), Female $<$ 40yo, Male $\geq$ 40yo, and Female $\geq$ 40yo. To evaluate differences in regional group-wide cDTI metrics compared to the global group-wide median, American Heart Association (AHA) segments were identified and unpaired t-tests with Bonferroni correction were used to detect significance between individual regions and the global group-wide median. We found no significant differences in global MD, FA, and HAP between age- and sex-based groups. Regional analysis revealed some significant differences compared to global group-wide cDTI metrics as well as in a few regions in group-specific comparisons. Overall, this study establishes baseline cDTI metrics in healthy subjects, providing a normative reference for assessing changes in cDTI metrics.

Keywords: Cardiac Diffusion Tensor Imaging · Microstructure · Tissue Characterization · Cardiac MRI

1 Introduction

Cardiac Diffusion Tensor Imaging (cDTI) is a magnetic resonance imaging (MRI) technique that encodes the Brownian motion of water molecules in order to probe myocardial mesostructure[29]. cDTI characterizes mesoscale cardiomyocyte orientation and organization, which can change during aging and disease[14,8]. cDTI metrics are obtained by acquiring several diffusion-weighted images (DWI) with diffusion sensitivity along different directions and then constructing the diffusion-tensor, which characterizes the principal directions and magnitudes of myocardial diffusion within each pixel. Mean diffusivity (MD) reflects the magnitude of water diffusion[3] in $\mu m^2/ms$. Fractional Anisotropy indicates the normalized ([0,1], unitless) magnitude of diffusive anisotropy and reflects the degree of cardiomyocyte organization[23]. Projecting the primary eigenvector of the diffusion tensor onto the epicardial tangent plane yields the helix angle (HA)[24,25], representing the angular orientation of cardiomyocytes relative to a local circumferential direction[18] in degrees.

As cDTI is an emerging technology, it is important to establish healthy baseline values for key cDTI metrics, including MD, FA and HA. It is also useful to describe how these values may change based on key biometric measures such as age, sex, BMI, and left-ventricular mass (LVM). Previous works have assessed average global or whole-slice (basal, mid-ventricular, apical) cDTI metrics[26] from three to five slices using stimulated echo acquision mode (STEAM)[20] and spin-echo sequences[5] and very few studies report on biometric effects other than age and sex. As the acquisition and post-processing continues to evolve, it is necessary to re-characterize these baselines with whole heart coverage, particularly for spin-echo acquisitions for which the data is not currently available.

The purpose of this work was to assess global and regional left ventricular cDTI metrics as a function of age and sex in a large cohort of healthy subjects. We hypothesize that there are no significant differences in cDTI metrics in this cohort of healthy subjects for global and regional group-wide and group-specific comparisons for cDTI metrics.

2 Methods

2.1 Image Acquisition and Post-Processing

Forty-six (N=46) healthy subjects signed statements of informed consent under IRB approval (Stanford Administrative Panel on Human Subjects in Medical Research, Reference #FWA00000929 & #FWA00000934), and underwent a cardiac exam using a 3T MRI (Vida Fit, Siemens) with an 18-channel body coil and 32-channel spine coil. A free-breathing, $M_0M_1M_2$ compensated, slice-following[21], single-shot, spin-echo echo-planar imaging acquisition was used to acquire cDTI data with the following parameters: resolution = $2\times2\times8$ mm^3, FOV = 256×256, Acceleration = GRAPPA$\times2$ [11], TE = 91ms, TR = 3R-R intervals, bandwidth = 1776Hz/Pixel, echo-spacing = 0.65ms, diffusion directions = 15, b = $350 s/mm^2$ and one b = 0 s/mm^2, averages = 10 (5 blip-up + 5

blip-down phase polarities), full LV-coverage (N_{slices} = 6-9, 0% Slice Gap), ∼2 minutes and 40 seconds per slice. This acquisition was ECG-gated to acquire images at one mid-systolic cardiac timepoint (Trigger Time = 285.2 ± 11.2 ms). Slices were acquired in an interleaved manner, such that odd-numbered slices were acquired first followed by even-numbered slices.

Images were then post-processed with the Cardiac Diffusion in Python (CarDpy) toolbox that calls the DiPy[10] utilities. This included Gibb's Ringing removal[13], shot-rejection, and respiratory sorting prior to distortion correction[2,6] between the blip-up and blip-down averages. After distortion correction, data was registered and then filtered by discarding pixels with computed MD greater than $3\mu m^2/ms$ (free water). Magnitude images were then averaged, denoised via Local PCA[19] and interpolated to a $1\times1\times8mm^3$ resolution. A non-linear least squares diffusion tensor reconstruction[17] was then applied to the data. Left ventricular segmentation, and the anterior and inferior right ventricular insertion points (RVIP) were manually identified via a custom graphical user interface (GUI) in which an averaged DWI from all directions (DWI_{avg}), MD map, and primary eigenvector map ($\boldsymbol{e_1}$) were used to delineate epicardial and endocardial borders. Global MD and FA were computed by averaging the metric across all pixels in the LV masks per subject. To compute the HA, the $\boldsymbol{e}_1$ in the masked LV region was projected onto the circumferential-longitudinal plane. An unwrapping filter was then applied to the helix angle maps. The helix angle pitch (HAP) was determined by linear regression of the pixel-wise HA values as a function of the normalized transmural wall thickness from endocardium (= 0) to epicardium (= 1). The normalized slope was reported as the HAP (°/% Thickness). The LVM was computed by multiplying the myocardial tissue density (1.053g/ml [28]) by the LV volume obtained after summing the LV masked pixels for all slices per subject. Slices were then identified as basal mid-ventricular or apical. The LV mask, RVIPs, and slice positions were used to define the regional American Heart Association 16-Segment Model[4].

2.2 Statistical Analysis

Group-wide and Group-specific Global Comparisons. Data were assessed using group-wide (all subjects) and group-specific cohorts. Four group-specific cohorts were defined as: (1) Males $<$ 40yo, (2) Females $<$ 40yo, (3) Males $\geq$ 40yo, and (4) Females $\geq$ 40yo. Significant differences ($p < 0.05$) in LVM, BMI, and diffusion metrics including MD, FA, and HAP between the four groups were assessed. For each metric, the normality of the group-specific distributions was first tested using the Shapiro-Wilk test. If all group-specific distributions were normally distributed, a one-way ANOVA was performed, followed by Tukey's HSD (honestly significant difference) *post hoc* test, if significant differences were detected. For non-normally distributed data, the Kruskal-Wallis test was applied, followed by Dunn's test with Bonferroni correction for *post hoc* analysis. Median group-wide and group-specific MD, FA, and HAP and the bootstrapped 95% confidence interval were reported.

Group-wide and Group-Specific Regional Comparisons. For regional analysis, AHA segmentation masks were applied to compute the average cDTI metric per segment for each volunteer. For each cDTI metric and segment, independent t-tests were performed to assess statistical significance ($p < 0.05$) between an AHA segment value and the global group-wide median. The median cDTI metric for each region was then plotted in a bullseye plot, with bold segments indicative of significant differences from the group-wide median.

For each AHA segment, volunteers were grouped into the same sub-groups as *Group-Specific* Global Comparisons in the previous section to enable evaluation of significant differences between groups on a regional level. For each region, significant ($p < 0.05$) differences were evaluated as above. Results of statistical tests were reported using a heat map and significantly different groups identified in *post hoc* testing were reported.

Table 1. Demographics of healthy subject cohort.

Demographics ($\mu \pm \sigma$)	subjects (#)	Age (years)	LVM (g)	BMI (kg/m^2)
Male $<$ 40 yo	11	28.6 ± 2.8	135.6 ± 29.1	24.0 ± 1.8
Female $<$ 40 yo	12	27.3 ± 3.8	80.4 ± 11.2	20.7 ± 2.4
Male $\geq$ 40 yo	11	49.4 ± 7.9	106.8 ± 27.9	24.1 ± 2.2
Female $\geq$ 40 yo	12	52.3 ± 7.8	75.9 ± 7.5	24.8 ± 3.5
Group-wide	46	39.4 ± 13.1	98.7 ± 31.4	23.4 ± 3.0

3 Results

3.1 Demographics

Demographics of the subject cohort are reported in Table 1. Male subjects $<$ 40yo had significantly greater LVM than female subjects $<$ 40yo ($p = 0.004$) and female subjects $\geq$ 40yo ($p < 0.001$). Male subjects $\geq$ 40yo had significantly greater LVM than both female subjects $<$ 40yo ($p = 0.04$) and female subjects $\geq$ 40yo ($p = 0.004$). Differences in BMI were also significant between females $<$ 40yo and all other groups: females $\geq$ 40yo (p = 0.002), males $<$ 40yo ($p = 0.02$) and males $\geq$ 40yo ($p = 0.01$).

3.2 Group-Wide and Group-Specific Comparisons

Adequate image quality was maintained across all slices (Fig. 1). Group-specific distributions of cDTI metrics exhibited some variability (Fig. 1). Median MD for females trended higher than males, while females <40yo tended to have steeper (more negative) HAP. However, no significant differences were observed between the groups. The median values of each metric for group-wide and group-specific populations are reported in Table 2. Box plots of the group-specific median values are shown in Fig. 2.

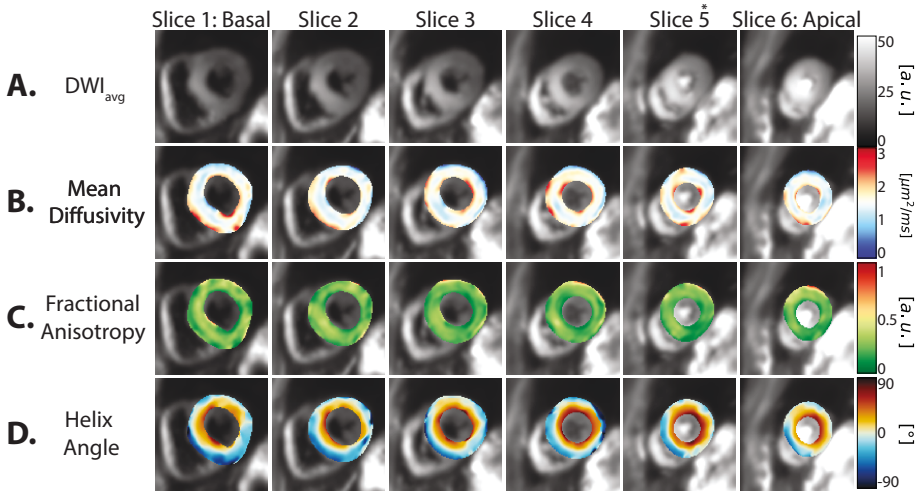

Fig. 1. Full left ventricular cDTI coverage demonstrated in a 40yo male subject. Images show the average DWI (DWI_{avg}) (A), MD (B), FA (C), and HA (D) maps with columns indicating the slice number and position (basal, mid-ventricular, and apical). Consistent image quality was observed across the acquired slices.

Table 2. Group-wide and group-specific global cDTI Metrics.

cDTI Metrics median [95% CI]	Mean Diffusivity [μm^2/ms]	Fractional Anisotropy [(0,1), unitless]	Helix Angle Pitch [°/%]
Male $<$ 40 yo	1.59 [1.48, 1.69]	0.26 [0.22, 0.28]	-0.85 [-0.91, -0.68]
Female $<$ 40 yo	1.64 [1.60, 1.86]	0.24 [0.23, 0.25]	-0.76 [-0.90, -0.60]
Male $\geq$ 40 yo	1.63 [1.55, 1.80]	0.25 [0.22, 0.27]	-0.70 [-0.90, -0.60]
Female $\geq$ 40 yo	1.65 [1.54, 1.79]	0.24 [0.21, 0.27]	-0.70 [-0.85, -0.57]
Group-wide	1.63 [1.51, 1.85]	0.25 [0.21, 0.28]	-0.77 [-0.92, -0.56]

3.3 Group-wide and Group-Specific Regional Comparisons.

The group-wide healthy subject analysis showed several significantly different regions compared to the group-wide median for MD, FA, and HAP (3). Basal regions tended to have more significant differences while the mid-ventricular and apical regions were more consistent. MD exhibited the most significantly different regions. This included: Segment-3, Segment-5 (Basal Inferolateral), Segment-7 (Mid-ventricular Anterior), Segment-8 (Mid-ventricular Anteroseptal), Segment-9 (Mid-ventricular Inferoseptal), and Segment-13 through Segment-16 (all apical segments). For FA, there were only three statistically significant segments: Segment-5 (Basal Inferolateral), Segment-11 (Mid-ventricular inferolateral), and Segment-14 (Apical Septal). For HAP, statistically significant segments included Segment-4 (Basal Inferior), Segment-5 (Basal Inferolateral), Segment-6 (Basal Anterolateral), Segment-10 (Mid-ventricular inferior), and Segment-16 (Apical

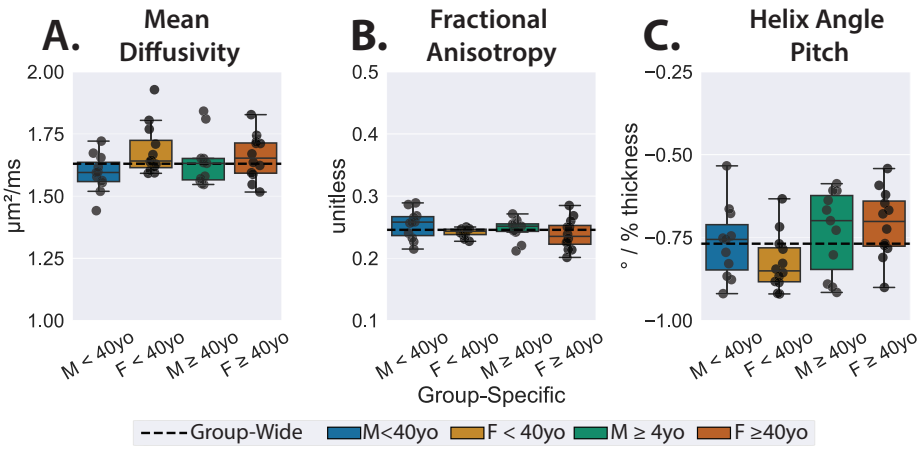

Fig. 2. Box plots of group-specific global median MD (A), FA (B), and HAP (C) for the subjects grouped by age and sex. Individual data points represent global median for an individual subject while the box plot represents the group-specific median metric and quartiles. The group-wide median is indicated by a dotted line. Although distributions had different trends between groups, no significant differences were observed in statistical analysis.

Lateral). Only Segment-5 (Basal Inferolateral) was significantly different from the global group-wide median for all three cDTI metrics (MD, FA, and HAP).

Results of group-specific regional statistical testing are shown in Fig. 3D. Overall, within a particular AHA-segment, age-sex sub-groups were generally not statistically different from one another with the exception of four segments. In Segment-4 (Basal Inferior), the HAP was significantly different between female subjects <40yo and Female subjects ≥40yo ($p = 0.0012$) and between female subjects <40yo and male subjects ≥ 40yo. In Segment-5 (Basal Inferolateral), the MD was significantly different between Females <40yo and Males <40yo ($p = 0.011$). In Segment-10 (Mid-ventricular Inferior), the MD was significantly different between Females ≥40yo and Males ≥40yo. In Segment-14 (Apical Septal), the Kruskal-Wallis test reported overall differences between groups ($p = 0.048$), but the Dunn's test in *post hoc* analysis did not reveal any pairwise statistically significant differences.

4 Discussion

In this study we investigated global and regional group-wide and group-specific differences for several cDTI metrics, including MD, FA, and HAP. We first categorized subjects into four groups based on age and sex, detecting no significant differences between the four groups globally. However, group-wide regional anal-

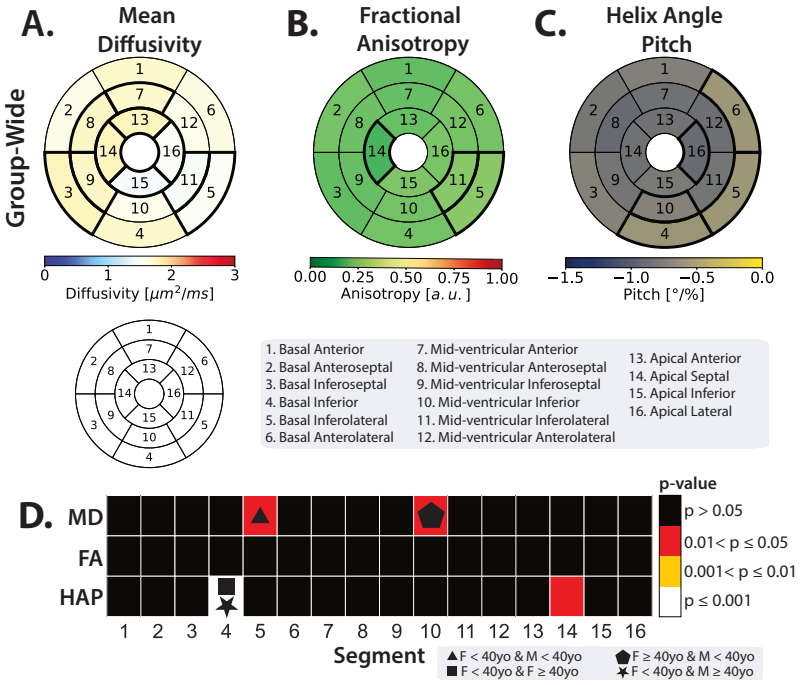

Fig. 3. Regional group-wide analysis for MD (A), FA (B), and HAP (C) and regional group-specific statistical analysis (D). In (A-C), bold segments indicate significant differences from the median group-wide global metric. Different cDTI metrics had different regions identified as significantly different compared to the group-wide global metric. MD had many more significantly different regions than FA and HAP. Segment-5 (Basal Inferolateral) was significantly different for all three metrics. Group-specific differences were generally not detected on a regional level with the exception of four segments.

ysis revealed that there were differences between segments and the global median for all three cDTI metrics. MD had the most statistically significant segments for group-wide regional analysis. There were also a few cases of group-specific regional differences. Therefore, our hypothesis was generally correct: global group-specific cDTI metrics did not differ between subjects, but some significant differences were observed in group-wide and group-specific regional assessments.

The lack of significant differences in cDTI metrics in group-specific global analysis may be attributed to the limitations of categorical grouping. Dividing age, a continuous variable, into arbitrary bins can hide subtle differences. We configured these groupings based on our inclusion criteria for the study, in which we targeted 10 subjects in each age-sex group. The small group sizes may further reduce statistical power, limiting the ability to detect meaningful significant trends. Using statistical analysis with higher power, such as a linear regression, would allow us to see if there are actual significant trends as a function of age

and sex. Some of these differences may have started to appear in the regional group-specific analysis, in which four AHA segments had statistically significant differences between groups. Although the total population in this study (N=46) exceeds typical cDTI cohorts, expanding the subject pool would help determine whether any physiologically-relevant statistical differences emerge.

The ranges of MD, FA, and HAP were similar to previously reported values. The range of MD values reported in this study are in the upper range of values typically reported in the literature (1.22 - 1.68 $\mu m^2/ms$)[7]. The FA values reported in our study were in the lower range of values typically reported in the literature (0.22 - 0.58 unitless)[7]. The reported HAP is shallower than the reported typical value (-1 $\pm$ 0.06 °/% thickness). Younger subjects trended towards steeper (more negative) HAP, which may be attributed to both age differences and more reliable cDTI data quality. The lower FA reported in our study may be from pseudo-diffusion effects as we used a non-diffusion weighted image as our reference low b-value image[7]. It has also been observed that distorted data exhibits a higher FA [6].

E2A (the angle between the projection of the second eigenvector on the cross-myocyte plane and the cross-myocyte direction perpendicular to the radial direction – see, e.g., [9,29]), is an additional cDTI metric that is often reported and relates to the orientation of myocardial sheetlets [7,22]. Herein, E2A was not reported because this metric is not sensitively encoded with motion-compensated spin-echo acquisitions in comparison to STEAM [15,26]. This is likely due to the longer diffusion "mixing" time of STEAM, in which diffusion encoding occurs over two heartbeats[16]. The longer time between the paired diffusion encoding gradients of STEAM likely enables spins to probe larger length scales, potentially improving sensitivity to sheetlets and the calculation of secondary eigenvectors. Similarly, spin-echo cDTI has been shown to have significantly higher uncertainties [1] in the secondary and tertiary eigenvectors compared to the primary eigenvector. As a result, E2A computations based on these eigenvectors are inherently more uncertain.

Regional differences were observed in group-wide data for all cDTI metrics. Basal segments were often statistically different, with Segment-5 (Basal Inferolateral) significantly different for each cDTI metric. The inferior and anterior walls of the heart experience more off-resonance from the air tissue interfaces of the heart, lungs, and liver. While distortion correction may mitigate some of these effects, it may not entirely mitigate data corruption. Additionally, base-to-apex shortening during contraction may contribute to complex, uncompensated motion corruption, resulting in less reliable diffusion encoding at basal slices. cDTI acquisition methods continue to evolve and this problem could be resolved with ultra-high-performance gradient system hardware (e.g., $G_{max} = 200$ mT/m, $S_{max} = 200$ T/m/s).

One limitation in this study is that the spin-echo acquisition approach currently leads to reliable cDTI metrics only in systole. This is, in part, a consequence of using widely available commodity MRI gradient hardware ($G_{max} = 45$ mT/m, $S_{max} = 200$ T/m/s). The use of a STEAM sequence for diffusion encod-

ing may enable more reliable data acquired in diastole[20]. Furthermore, utilizing ultra-high-performance gradient hardware may enable higher SNR and potentially more reliable systolic and diastolic data with spin-echo cDTI.

The normative values in this study may also only hold for this protocol and hardware. We would need to investigate if MD, FA, and HAP would change if we move to ultra-high-performance hardware (e.g., $G_{max} = 200$ mT/m, $S_{max} = 200$ T/m/s). A recent work[12] suggests that moving to advanced hardware reduces MD, maintains FA, and increases the steepness of the HAP while reducing the variation in these metrics. We would therefore expect similar trends in our data; however, the relative trends in our study between group-wide and group-specific comparisons would likely be consistent. Likewise, we would expect a decrease in the uncertainty[1] of cDTI metrics with advanced hardware, which would allow us to investigate smaller variations in cDTI metrics not only within a healthy volunteer cohort but also in comparing this population to patients.

Future work would investigate the effects of BMI, LV mass, R-R interval, LV ejection fraction, end-diastolic volume, and end-systolic volume on the cDTI metrics both globally and regionally. We also plan to assess the relationship between the cDTI metrics and cardiac strains computed from Cine DENSE (displacement encoding with stimulated echoes)[27] MR acquisition. Furthermore, the baseline cDTI metrics defined in this study can also serve to evaluate microstructural changes in cardiovascular disease that use the same protocol.

5 Conclusion

We characterized global cDTI metrics (MD, FA, and HAP) in a cohort of healthy subjects. No significant differences in age-sex groups were found for global metrics, but a few regions showed significant differences between groups. Several significant global regional differences were observed when compared to the group-wide median, suggesting there may be subtle regional variations in the healthy population. This study provides cDTI metric trends in healthy subjects, offering a reference for using cDTI to characterize microstructure.

Acknowledgments. This study was supported, in part, by AHA 23PRE1018442 to AJH, NIH R01-HL152256 and NSF 2205103 to DBE, and NSF 2205043 to LEP.

Disclosure of Interests. The authors have no competing interests to declare that are relevant to the content of this article.

Accepted Version This version of the contribution has been accepted for publication, after peer review but is not the Version of Record and does not reflect post-acceptance improvements, or any corrections. The Version of Record is available online at: http://dx.doi.org/10.1007/978-3-031-94562-5_17. Use of this Accepted Version is subject to the publisher's Accepted Manuscript terms of use https://www.springernature.com/gp/open-research/policies/accepted-manuscript-terms.

References

1. Aliotta, E., Moulin, K., Magrath, P., Ennis, D.B.: Quantifying precision in cardiac diffusion tensor imaging with second-order motion-compensated convex optimized diffusion encoding. Magnetic Resonance in Medicine **80**(3), 1074–1087 (2018). https://doi.org/10.1002/mrm.27107
2. Andersson, J.L.R., Skare, S., Ashburner, J.: How to correct susceptibility distortions in spin-echo echo-planar images: application to diffusion tensor imaging. NeuroImage **20**(2), 870–888 (2003). https://doi.org/10.1016/S1053-8119(03)00336-7
3. Basser, P.J., Mattiello, J., LeBihan, D.: Estimation of the effective self-diffusion tensor from the NMR spin echo. Journal of Magnetic Resonance B **103**(3), 247–254 (1994). https://doi.org/10.1006/jmrb.1994.1037
4. Cerqueira, M.D., Weissman, N.J., Dilsizian, V., Jacobs, A.K., Kaul, S., Laskey, W.K., Pennell, D.J., Rumberger, J.A., Ryan, T., Verani, M.S.: Standardized myocardial segmentation and nomenclature for tomographic imaging of the heart. Circulation **105**(4), 539–542 (2002). https://doi.org/10.1161/hc0402.102975
5. Chen, S., Kara, D., Garrett, T., Orlandi, P., Kwon, D., Nguyen, C.: Characterization of myocardial microstructure using DT-CMR with ultra-high-performance gradient scanner in healthy subjects. In: Proceedings of the International Society for Magnetic Resonance in Medicine (ISMRM) 2024 (May 2024), https://ismrm.org/2024, conference abstract
6. Coll-Font, J., Chen, S., Eder, R., Fang, Y., Han, Q.J., van den Boomen, M., Sosnovik, D.E., Mekkaoui, C., Nguyen, C.T.: Manifold-based respiratory phase estimation enables motion and distortion correction of free-breathing cardiac diffusion tensor MRI. Magnetic Resonance in Medicine **87**(1), 474–487 (2022). https://doi.org/10.1002/mrm.28972
7. Dall'Armellina, E., Ennis, D.B., Axel, L., Croisille, P., Ferreira, P.F., Gotschy, A., Lohr, D., Moulin, K., Nguyen, C.T., Nielles-Vallespin, S., Romero, W., Scott, A.D., Stoeck, C., Teh, I., Tunnicliffe, E.M., Viallon, M., Wang, V., Young, A.A., Schneider, J.E., Sosnovik, D.E.: Cardiac diffusion-weighted and tensor imaging: A consensus statement from the special interest group of the society for cardiovascular magnetic resonance. Journal of Cardiovascular Magnetic Resonance **27**(1) (2025). https://doi.org/10.1016/j.jocmr.2024.101109
8. Das, A., Kelly, C., Teh, I., Stoeck, C.T., Kozerke, S., Sharrack, N., Swoboda, P.P., Greenwood, J.P., Schneider, J.E., Plein, S., Dall'Armellina, E.: Pathophysiology of LV Remodeling Following STEMI: A Longitudinal Diffusion Tensor CMR Study. JACC: Cardiovascular Imaging **16**(2), 159–171 (Feb 2023). https://doi.org/10.1016/j.jcmg.2022.04.002
9. Ferreira, P.F., Kilner, P.J., McGill, L.A., Nielles-Vallespin, S., Scott, A.D., Ho, S.Y., McCarthy, K.P., Haba, M.M., Ismail, T.F., Gatehouse, P.D., et al.: In vivo cardiovascular magnetic resonance diffusion tensor imaging shows evidence of abnormal myocardial laminar orientations and mobility in hypertrophic cardiomyopathy. Journal of Cardiovascular Magnetic Resonance **16**(1), 87 (2014)
10. Garyfallidis, E., Brett, M., Amirbekian, B., Rokem, A., Van Der Walt, S., Descoteaux, M., Nimmo-Smith, I., Contributors, D.: Dipy, a library for the analysis of diffusion MRI data. Frontiers in Neuroinformatics (February 2014). https://doi.org/10.3389/fninf.2014.00008
11. Griswold, M.A., Jakob, P.M., Heidemann, R.M., Nittka, M., Jellus, V., Wang, J., Kiefer, B., Haase, A.: Generalized autocalibrating partially parallel acquisitions (grappa). Magnetic Resonance in Medicine **47**(6), 1202–1210 (2002). https://doi.org/10.1002/mrm.10171

12. Kara, D., Liu, Y., Chen, S., Garrett, T., Younis, A., Sugawara, M., Bolen, M.A., Bi, X., Wazni, O., Nakagawa, H., Kwon, D., Nguyen, C.: In vivo cardiac diffusion tensor imaging on an mr system featuring ultrahigh performance gradients with 200 mt/m maximum gradient strength. Magnetic Resonance in Medicine **93**(2), 673–688 (September 2024). https://doi.org/10.1002/mrm.30308
13. Kellner, E., Dhital, B., Kiselev, V.G., Reisert, M.: Gibbs-ringing artifact removal based on local subvoxel-shifts. Magnetic Resonance in Medicine **76**(5), 1574–1581 (2016). https://doi.org/10.1002/mrm.26054
14. Khalique, Z., Ferreira, P.F., Scott, A.D., Nielles-Vallespin, S., Firmin, D.N., Pennell, D.J.: Diffusion tensor cardiovascular magnetic resonance imaging: A clinical perspective. JACC: Cardiovascular Imaging **13**(5), 1235–1255 (2020). https://doi.org/https://doi.org/10.1016/j.jcmg.2019.07.016
15. Khalique, Z., Scott, A.D., Ferreira, P.F., Nielles-Vallespin, S., Firmin, D.N., Pennell, D.J.: Diffusion tensor cardiovascular magnetic resonance in hypertrophic cardiomyopathy: a comparison of motion-compensated spin echo and stimulated echo techniques. MAGMA **33**(3), 331–342 (2019). https://doi.org/10.1007/s10334-019-00799-3
16. Kim, S., Chi-Fishman, G., Barnett, A.S., Pierpaoli, C.: Dependence on diffusion time of apparent diffusion tensor of ex vivo calf tongue and heart. Magnetic Resonance in Medicine **54**(6), 1387–1396 (2005). https://doi.org/10.1002/mrm.20676
17. Kingsley, P.B.: Introduction to diffusion tensor imaging mathematics: Part iii. tensor calculation, noise, simulations, and optimization. Concepts in Magnetic Resonance Part A **28**(2), 155–179 (2006). https://doi.org/10.1002/cmr.a.20057
18. Lombaert, H., Peyrat, J.M., Croisille, P., Rapacchi, S., Fanton, L., Cheriet, F., Clarysse, P., Magnin, I., Delingette, H., Ayache, N.: Human atlas of the cardiac fiber architecture: study on a healthy population. IEEE Transactions on Medical Imaging **31**(7), 1436–1447 (2012). https://doi.org/10.1109/TMI.2012.2192743
19. Manjón, J.V., Coupé, P., Concha, L., Buades, A., Collins, D.L., Robles, M.: Diffusion weighted image denoising using overcomplete local PCA. PLoS One **8**(9), e73021 (2013). https://doi.org/10.1371/journal.pone.0073021
20. McGill, L.A., Ferreira, P.F., Scott, A.D., Nielles-Vallespin, S.: Relationship between cardiac diffusion tensor imaging parameters and anthropometrics in healthy volunteers. Journal of Cardiovascular Magnetic Resonance **18**(2) (2016). https://doi.org/10.1186/s12968-015-0215-0
21. Moulin, K., Croisille, P., Feiweier, T., Delattre, B.M.A., Wei, H., Robert, B., Beuf, O., Viallon, M.: In vivo free-breathing DTI and IVIM of the whole human heart using a real-time slice-followed SE-EPI navigator-based sequence: A reproducibility study in healthy volunteers. Magnetic Resonance in Medicine **76**(1), 70–82 (2016). https://doi.org/10.1002/mrm.25852
22. Moulin, K., Verzhbinsky, I.A., Maforo, N.G., Perotti, L.E., Ennis, D.B.: Probing cardiomyocyte mobility with multi-phase cardiac diffusion tensor mri. PLOS ONE **15**(11), e0241996 (November 2020). https://doi.org/10.1371/journal.pone.0241996
23. Pierpaoli, C., Basser, P.J.: Toward a quantitative assessment of diffusion anisotropy. Magnetic Resonance in Medicine **36**(6), 893–906 (1996). https://doi.org/10.1002/mrm.1910360612
24. Reese, T.G., Weisskoff, R.M., Smith, R.N., Rosen, B.R., Dinsmore, R.E., Wedeen, V.J.: Imaging myocardial fiber architecture in vivo with magnetic resonance. Magnetic Resonance in Medicine **34**(6), 786–791 (1995). https://doi.org/10.1002/mrm.1910340603

25. Scollan, D.F., Holmes, A., Winslow, R., Forder, J.: Histological validation of myocardial microstructure obtained from diffusion tensor magnetic resonance imaging. American Journal of Physiology-Heart and Circulatory Physiology **275**(6), H2308–H2318 (1998). https://doi.org/10.1152/ajpheart.1998.275.6.H2308
26. Scott, A.D., Nielles-Vallespin, S., Ferreira, P.F., Khalique, Z., Gatehouse, P.D., Kilner, P., Pennell, D.J., Firmin, D.N.: An in-vivo comparison of stimulated-echo and motion compensated spin-echo sequences for 3 T diffusion tensor cardiovascular magnetic resonance at multiple cardiac phases. Journal of Cardiovascular Magnetic Resonance **20**, 1 (2018). https://doi.org/10.1186/s12968-017-0425-8
27. Spottiswoode, B.S., Zhong, X., Hess, A.T., Kramer, C.M., Meintjes, E.M., Mayosi, B.M., Epstein, F.H.: Tracking myocardial motion from cine dense images using spatiotemporal phase unwrapping and temporal fitting. IEEE Transactions on Medical Imaging **26**(1), 15–30 (2007). https://doi.org/10.1109/TMI.2006.884215
28. Vinnakota, K.C., Bassingthwaighte, J.B.: Myocardial density and composition: a basis for calculating intracellular metabolite concentrations. American Journal of Physiology-Heart and Circulatory Physiology **286**(5), H1742–H1748 (2004). https://doi.org/10.1152/ajpheart.00478.2003
29. Wilson, A.J., Sands, G.B., LeGrice, I.J., Young, A.A., Ennis, D.B.: Myocardial mesostructure and mesofunction. American Journal of Physiology-Heart and Circulatory Physiology **323**(2), H257–H275 (2022). https://doi.org/10.1152/ajpheart.00059.2022